Practical Demonstration of Robust InSAR Optimization for Multipass InSAR

Yuanyuan, Wang, Signal Processing in Earth Observation, Technical University of Munich, wang@bv.tum.de, Germany

Xiao Xiang, Zhu, Signal Processing in Earth Observation, Technical University of Munich, and Remote Sensing Technology Institute, German Aerospace Center, xiao.zhu@dlr.de, Germany

Abstract

Multipass / multibaseline SAR interferometric measurements may suffer from, for example, non-Gaussian scatterers in the context of distributed scatterers, and unmodeled interferometric phase such as unmodeled motion phase and atmospheric phase. Robust InSAR Optimization (RIO) is a framework that systematically tackles these problems. Experiments show that RIO greatly outperform the current methods in terms of the variance of phase history parameter estimates for contaminated observations, but still keeps an relative efficiency of 80% when the observations are outlier-free.

1 Introduction

Multipass interferometric synthetic aperture radar (InSAR) techniques exploit time series signals of scatterers to measure the ground deformation as well as deformation of individual building and reconstruct urban 3-D infrastructure. For example persistent scatterer interferometry (PSI) [1], [2], SqueeSAR [3], [4], which utilizes persistent scatterers (PS) and distributed scatterers (DS), respectively. In general, millimeter accuracy of the yearly linear deformation rate and meter accuracy of the scatterer's 3-D position can be achieved with respect to a reference point [1], [5], [6].

However, this accuracie refer to the optimal estimators derived based on the assumption of Gaussian-distributed data. PS is modeled as a deterministic signal with additive zero-mean white complex circular Gaussian (CCG) noise [1], while DS is modeled as correlated zero-mean CCG [3], [7]. Violation of the assumptions greatly compromises the performance of the estimator, which can be boiled down to two fundamental categories in the parameter estimation of multipass InSAR:

- Unmodeled phase such as residual atmospheric/orbit phase errors, unmodeled motion phase, etc. Such phase errors impose non-Gaussian noise on PS and DS.
- Non-Gaussian scatterers that bias the covariance matrix estimation of DS. Their spatial stationarity cannot be guaranteed because of the spatially varying phase.

The Robust InSAR Optimization (RIO) framework [8] is designed not only but especially for dealing with such data. It introduces the following aspects in the current techniques:

- It replaces the maximum likelihood estimator (MLE) for Gaussian distribution which minimizes the sum of the squared residuals with an M-estimator [9] which minimizes the sum of a customized function $\rho(x)$ of the residuals.

- Should DS be exploited, the sample covariance matrix $\hat{\mathbf{C}}$ is replaced with the robust *rank M-estimator* (RME) of the covariance: $\hat{\mathbf{C}}_{RME}$ proposed in this paper. $\hat{\mathbf{C}}_{RME}$ is robust against both outlier and samples with non-stationary phase.

2 Robust InSAR Optimization

2.1 M-estimator Basics

M-estimators are a class of well-known robust estimators. It stands for MLE-type estimator, which allows minimizing a customized loss function $\rho(x)$ of the residuals to resist outliers without pre-processing the data such as outlier trimming. Let $f_{\mathbf{g}}(\mathbf{g})$ be a generic likelihood function of $\mathbf{g}$. Choosing $\rho = -\ln f_{\mathbf{g}}(\mathbf{g})$ gives the MLE for $f_{\mathbf{g}}(\mathbf{g})$. The MLE under the Gaussian distribution assumption corresponds to an M-estimator with $\rho(x) = x^2$. For a linear system, its M-estimator can in general be solved by iteratively re-weighted least square, with the weights of each observation being

$$w(\varepsilon_i) = \rho'(\varepsilon_i)/\varepsilon_i \qquad (2.1)$$

The M-estimator is a trade-off between efficiency and robustness. However, it can still maintain high efficiency under the nominal model by properly choosing the loss function or weighting function. Popular weighting

functions are Tukey's biweight function, t-distribution weighting functions, and so on.

2.2 Robust Phase History Parameter Estimators

2.2.1 Persistent Scatterers

One of the commonly used estimators for PS phase history parameters $\boldsymbol{\theta}$ is the periodogram:

$$\hat{\boldsymbol{\theta}} = \arg\max_{\boldsymbol{\theta}} \left\{ \left\| N^{-1} \sum_{n=1}^{N} g_n \exp\left(-j\varphi_n(\boldsymbol{\theta})\right) \right\| \right\} \quad (2.2)$$

The g_n and φ_n are the complex pixel value and the modeled phase of the nth image, respectively. Equation (2.2) is actually the MLE under the assumption of additive i.i.d. CCG noise [10].

Assuming Gaussian noise for PS is well justified. However, the uncompensated phase error especially atmospheric phase renders the noise of PS no longer Gaussian. Therefore, we proposed the following estimator to deal with possible large phase error:

$$\hat{\boldsymbol{\theta}} = \arg\min_{\boldsymbol{\theta}} \sum_{i=1}^{N} \rho\left(\frac{\mathrm{Re}\left[\varepsilon_i(\boldsymbol{\theta})\right]}{\sigma_R}\right) + \rho\left(\frac{\mathrm{Im}\left[\varepsilon_i(\boldsymbol{\theta})\right]}{\sigma_I}\right) \quad (2.3)$$

where the residual $\varepsilon_i(\boldsymbol{\theta})$ is $g_i - \exp\left(-j\varphi_i(\boldsymbol{\theta})\right)$, $\mathrm{Re}[\bullet$, $\mathrm{Im}[\bullet$ are the real and imaginary parts, and σ_R and σ_I are the standard deviations of the real and imaginary parts, respectively. Equation (2.3) is solved iteratively, where σ_R and σ_I are updated at each iteration.

2.2.2 Distributed Scatterers

If stationarity is assumed for the DS and its neighbourhood, one can treat the DS neighbourhood as a single PS by averaging all the DS pixels in the neighbourhood, like SqueeSAR. The robustified estimator is simply identical to equation (2.3). However, stationarity is not assumes in our considerations. We aim at a full inversion of individual DS pixel. The original MLE introduced in [11] is recalled here:

$$\hat{\boldsymbol{\theta}} = \arg\min_{\boldsymbol{\theta}} \left\{ \mathbf{g}^H \boldsymbol{\Phi}(\boldsymbol{\theta}) \left|\hat{\mathbf{C}}\right|^{-1} \boldsymbol{\Phi}(\boldsymbol{\theta})^H \mathbf{g} \right\} \quad (2.4)$$

where $\boldsymbol{\Phi}(\boldsymbol{\theta})$ is the diagonal matrix containing the modelled phase of $\mathbf{g}$, and $|\bullet$ is the matrix element-wise absolute value operator. The robustified DS estimator follows the same expression as equation (2.4). Written into a matrix form, it is:

$$\hat{\boldsymbol{\theta}} = \arg\min_{\boldsymbol{\theta}} \left\{ \boldsymbol{\varepsilon}^H(\boldsymbol{\theta}) \mathbf{W} \boldsymbol{\varepsilon}(\boldsymbol{\theta}) \right\} \quad (2.5)$$

where $\mathbf{W}$ is a diagonal weighting matrix as a function of the residuals $\boldsymbol{\varepsilon}(\boldsymbol{\theta})$. The residual is the whitened observations, i.e.

$$\boldsymbol{\varepsilon}(\boldsymbol{\theta}) = \left|\hat{\mathbf{C}}\right|^{-1/2} \boldsymbol{\Phi}(\boldsymbol{\theta})^H \mathbf{g} \quad (2.6)$$

The residual is better to be whitened with a robust covariance matrix estimate, such as the $\hat{\mathbf{C}}_{RME}$ which will be covered in Section 2.3.2.

One should be aware that the marginal distribution of the phase of zero mean CCG multivariate is uniform, as well as its whitened version. The atmospheric phase, presumably also uniformly distributed over time, applies no change to the DS observations statistically. In another word, the robust loss function is blind to such phase contamination on a single-look DS observation.

Therefore, the corrected weighting on the contaminated observations has to be introduced to the estimator. The weights should be calculated based on the expected residuals $\bar{\boldsymbol{\varepsilon}}$ of the whole DS neighbourhood. The expected residual must be robustly estimated as (2.7), due to the possible outliers in the neighbourhood:

$$\bar{\boldsymbol{\varepsilon}} = \left(\sum_{m=1}^{M} w^m\right)^{-1} \sum_{m=1}^{M} w^m \boldsymbol{\varepsilon}\left(\hat{\boldsymbol{\theta}}^m\right) \quad (2.7)$$

where the superscript m denotes the sample number in the neighbourhood, and w^m is a robust weight, e.g. Tukey's biweight. The complete final estimator should be as follows:

$$\hat{\boldsymbol{\theta}}^m = \arg\min_{\boldsymbol{\theta}^m} \left\{ \boldsymbol{\varepsilon}^H\left(\boldsymbol{\theta}^m\right) \mathbf{W}(\bar{\boldsymbol{\varepsilon}}) \boldsymbol{\varepsilon}\left(\boldsymbol{\theta}^m\right) \right\} \quad (2.8)$$

Similar to (2.3), equation (2.8) is solved iteratively. The weighting matrix is updated at each iteration. Its computation should start with a selected DS neighbourhood which jointly determines a single weighting matrix. This matrix is used for the parameters retrieval of each single-look DS observation vector in the neighbourhood. The weighting matrix is then updated according to all the estimates in the neighbourhood.

2.3 Robust Covariance Estimators

2.3.1 For Stationary Non-Gaussian Samples

If the selected samples are non-Gaussian, caused by either a non-Gaussian scattering mechanism or a poor sample selection, the covariance estimation can be robustified using an M-estimator. In this section, we assume the samples' stationarity on the phase, i.e. the expected interferometric phases are identical for all the samples.

The M-estimator of a covariance matrix is basically an iteratively reweighted sample covariance matrix [12]:

$$\hat{\mathbf{C}}_{k+1} = \frac{1}{M} \sum_{m=1}^{M} w\left(\varepsilon_m\left(\hat{\mathbf{C}}_k\right)\right) \mathbf{g}_m \mathbf{g}_m^H \quad (2.9)$$

where k is the iteration index, and $w(x)$ is a weighting function. $w(x)$ down-weights highly deviating samples

whose whitened version $\varepsilon_m\left(\hat{\mathbf{C}}_k\right)=\left\|\hat{\mathbf{C}}_k^{-1/2}\mathbf{g}_m\right\|$ is large, which greatly depends on the intensities of $\mathbf{g}_m$.

Equation (2.9) is solved iteratively. One engineering solution to drop the iteration is the sign covariance matrix [8], [13]:

$$\hat{\mathbf{C}}_{SCM} = N\,\bar{I}/M \cdot \sum_{m=1}^{M}\left\|\mathbf{g}_m\right\|^{-2}\mathbf{g}_m\mathbf{g}_m^{H} \qquad (2.10)$$

where $\bar{I}$ is the expected intensity, and N is the number of images.

2.3.2 Non-stationary Non-Gaussian Scatterer

For samples with non-stationary phase caused by topography, deformation, etc., we define a new quantity: complex *rank* of InSAR multivariate as follows [8]:

$$\hat{\mathbf{r}}_m = \frac{1}{J}\sum_{j=1}^{J}\mathbf{g}_m \bullet \qquad \bullet \quad , \qquad (2.11)$$

where $\mathbf{g}_j$ is the direct neighbourhood of $\mathbf{g}_m$, and the $\bullet$ denotes the element-wise product. Through the multiplication of the sample with the complex conjugate of its direct neighbour, the deterministic phase is mitigated.

Based on (2.11), we can define the RME of the covariance matrix analogous to (2.9) as follows [8]:

$$\hat{\mathbf{C}}_{RME} = \frac{1}{M}\sum_{m=1}^{M}w(\varepsilon_m)\hat{\mathbf{r}}_m\hat{\mathbf{r}}_m^{H}, \qquad (2.12)$$

where $\varepsilon_m^2 = \hat{\mathbf{r}}_m^{H}\hat{\mathbf{C}}^{-1}\hat{\mathbf{r}}_m$, and the iteration index k is dropped for simplicity. The RME is a fourth-order descriptor of the sample statistics. It can be proven that the element wise square root of $\left|\hat{\mathbf{C}}_{RME}\right|$ approaches $\left|\hat{\mathbf{C}}_{MLE}\right|$ asymptotically under CCG for using one direct neighbourhood [8]. Therefore, element-wise square root on $\left|\hat{\mathbf{C}}_{RME}\right|$ should be taken after equation (2.12).

3 Practical Demonstrations

This section will demonstrate the performance of RIO on real data. The readers can refer to [8] for numerous simulations on the estimators robustness and efficiencies at different outlier levels.

3.1 Robustness Against Unmodeled Phase

To demonstrate the robustness against large phase error, an area in Las Vegas with significant non-linear motion was selected, in a stack of 30 TerraSAR-X high resolution spotlight images. The test area is shown in Figure 1(a). As an example, the deformation phase history of the pixel marked by yellow cross w.r.t. a reference point nearby (few hundred meters away) is shown in Figure 1(b). As we can see, not only the motion is complex but also the magnitude of motion is very large. If only linear motion model is considered, the unmodeled motion

phase is equivalent to large phase error. Non-robust estimators will give biased estimates.

Figure 2(a) compares the result of the proposed robust estimator and the ordinary MLE when only the linear model is considered. The robust estimates correctly reconstruct the subsiding bowl, whereas the MLE estimates are heavily biased by the unmodeled motion of the building. The advantage of the robust estimator is clearer in Figure 2(b) which is the bias of the estimates w.r.t. the reference linear deformation rate estimated using a multi-component nonlinear motion model [14].
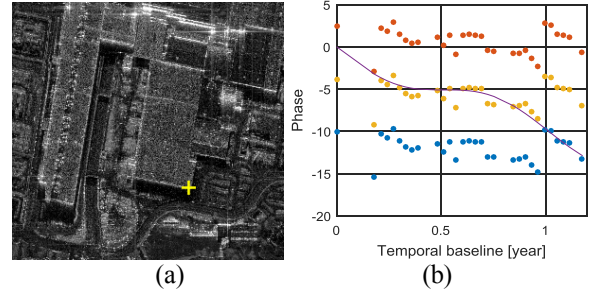

(a)   (b)

Figure 1. (a) the test area with significant non-linear motion is marked by the red rectangle. The red cross is the reference point. (b) the deformation phase history of the pixel marked by yellow cross in (a). The purple curve is a non-linear fit to the phase history.

3.2 Robustness against Non-Gaussian Scatterers

Figure 3 shows the linear deformation rate of the DSs estimated using the classical sample covariance matrix $\hat{\mathbf{C}}_{MLE}$ (left column) and that using the proposed $\hat{\mathbf{C}}_{RME}$ (right column). Identical samples were used for estimating these two covariance matrices. They were adaptively selected with the Kolmogorov-Smirnov (KS) test using ten amplitude images. Due to the low detection rate caused by the small number of images, we expect a non-negligible number of outliers in the selected samples. The same ordinary DS MLE was employed to estimate the linear deformation rate in both cases. Therefore, any improvement was solely credited to the use of a more robust covariance matrix estimate.

The improvement is clearly demonstrated. The test area is mainly vegetation, except a road in the center which usually appears as a DS in the X-band images. Homogeneous deformation rates are expected, as the spans of both areas were roughly one hundred meters. However, many estimates appear in subfigure (a) as salt-and-pepper noise. We believe this is due to the low detection rate of the KS test, and the non-stationarity of the samples. In contrast, homogenous deformation rate of the road is shown in subfigure (b).

For further comparison, the histograms of the linear deformation rates of the road were plotted in Figure 3 (c)

and (d) respectively. When using $\hat{\mathbf{C}}_{MLE}$, many local peaks appear in the histogram which should not correspond to the deformation signal. With $\hat{\mathbf{C}}_{RME}$, results are considerably more homogenous, and thus more reasonable.
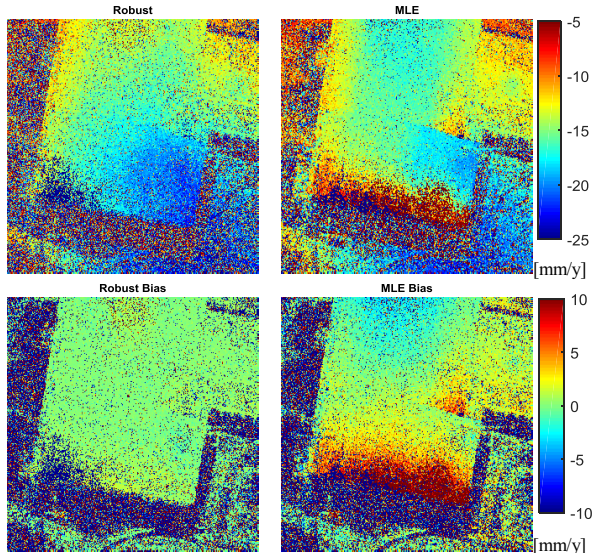

Figure 2. (a) linear deformation rate estimates by robust estimator and ordinary MLE, and (b) the bias of the robust and non-robust estimates to the "ground truth" (linear deformation rate estimated considering the nonlinear motion model). Unit: [mm/year].

Figure 3. (a) and (b) comparison of the linear deformation rate of the two test sites estimated using the ordinary $\hat{\mathbf{C}}_{MLE}$ and the proposed $\hat{\mathbf{C}}_{RME}$, respectively, and (c) and (d) the corresponding histograms of the linear deformation rates in Figure 3 (a) (b).

References

[1]   A. Ferretti, C. Prati, and F. Rocca, "Permanent scatterers in SAR interferometry," *IEEE Trans. Geosci. Remote Sens.*, vol. 39, no. 1, pp. 8–20, Jan. 2001.

[2]   N. Adam, B. Kampes, M. Eineder, J. Worawattanamateekul, and M. Kircher, "The development of a scientific permanent scatterer system," in *ISPRS Workshop High Resolution Mapping from Space, Hannover, Germany*, 2003, vol. 2003.

[3]   A. Ferretti, A. Fumagalli, F. Novali, C. Prati, F. Rocca, and A. Rucci, "A New Algorithm for Processing Interferometric Data-Stacks: SqueeSAR," *IEEE Trans. Geosci. Remote Sens.*, vol. 49, no. 9, pp. 3460–3470, Sep. 2011.

[4]   Y. Wang, X. Zhu, and R. Bamler, "Retrieval of Phase History Parameters from Distributed Scatterers in Urban Areas Using Very High Resolution SAR Data," *IS-PRS J. Photogramm. Remote Sens.*, vol. 73, pp. 89–99, Sep. 2012.

[5]   R. Bamler, M. Eineder, N. Adam, X. Zhu, and S. Gernhardt, "Interferometric Potential of High Resolution Spaceborne SAR," *Photogramm. - Fernerkund. - Geoinformation*, vol. 2009, no. 5, pp. 407–419, Nov. 2009.

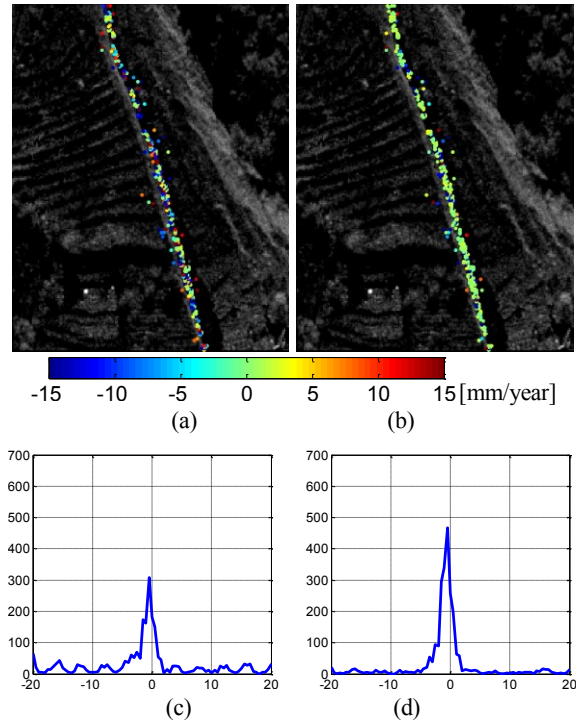[6]   X. Zhu and R. Bamler, "Very High Resolution Spaceborne SAR Tomography in Urban Environment," *IEEE*

Trans. Geosci. Remote Sens., vol. 48, no. 12, pp. 4296–4308, 2010.

[7]   R. Bamler and P. Hartl, "Synthetic aperture radar interferometry," *Inverse Probl.*, vol. 14, no. 4, p. R1, 1998.

[8]   Y. Wang and X. X. Zhu, "Robust Estimators for Multipass SAR Interferometry," *IEEE Trans. Geosci. Remote Sens.*, vol. 54, no. 2, 2015.

[9]   P. J. Huber, *Robust Statistics*. John Wiley & Sons, 1981.

[10]   D. Rife and R. R. Boorstyn, "Single tone parameter estimation from discrete-time observations," *Inf. Theory IEEE Trans. On*, vol. 20, no. 5, pp. 591–598, 1974.

[11]   F. De Zan and F. Rocca, "Coherent processing of long series of SAR images," in *Geoscience and Remote Sensing Symposium, 2005. IGARSS '05. Proceedings. 2005 IEEE International*, 2005, vol. 3, pp. 1987–1990.

[12]   E. Ollila and V. Koivunen, "Influence functions for array covariance matrix estimators," in *Statistical Signal Processing, 2003 IEEE Workshop on*, 2003, pp. 462–465.

[13]   S. Visuri, V. Koivunen, and H. Oja, "Sign and rank covariance matrices," *J. Stat. Plan. Inference*, vol. 91, no. 2, pp. 557–575, 2000.

[14]   X. X. Zhu and R. Bamler, "Let's Do the Time Warp: Multicomponent Nonlinear Motion Estimation in Differential SAR Tomography," *IEEE Geosci. Remote Sens. Lett.*, vol. 8, no. 4, pp. 735–739, 2011.